Swarm shape and its dynamics in a predator-swarm model

Hayley Tomkins[*] and Theodore Kolokolnikov[†]

November 25, 2014

Abstract

We consider a particle predator-swarm model introduced in [1]. In the continuum limit of many prey particles, we develop a numerical method which tracks the boundary of the swarm. We use this method to explore the variety and complexity of swarm shapes. We also consider a special limiting case where the predator is moving inside an infinite sea of prey. Two subcases are studied: one where the predator is moving along a straight line, and another where the predator is moving in a circle. Various topological changes in the swarm shape are observed as the predator speed is increased, such as the appearence of an infinite tail for a predator moving in a straight line when its speed is large enough.

1   Introduction

Recently there have been many attempts to produce swarm models that have both the accuracy and complexity to be meaningful and the simplicity to be subjected to analysis. Each model uses a slightly different approach. Some focus on specific animal groupings, such as shoals of fish, [2, 3, 4], flocks of birds, [5], and locust swarms, [6, 7, 8, 9]. Many propose an individual-based model, [10, 11, 8], while others opt to build their model based on collected data [12, 13, 14]. One approach used force matching to reverse engineer interactions [15]. In another approach, a game-like model is used [16]. Notably, some swarms are modeled by a Particle Swarm Optimization algorithm [17, 18]. In particular, we highlight the model proposed by Silva et. al. [19] who introduced a single predator to the algorithm, thus considering a similar situation as we explore in the following. More in-depth overviews of the approaches used in this field can also be found [20, 21], as well as overviews of the modeling approach itself [22].

The variability of these models is owed partially to the field from which the problem is approached; it is looked at from, most prominently, biology, mathematics, physics, and engineering [22]. Often the ultimate goal of these observations is to model changing populations numbers in between a group of predators and a linked group of prey [23]. Yet, despite these variations, recurring features exist between these models. Principally, there is commonly "a short-range repulsion, a longer-range attraction, and and/or an alignment among interacting agents" [2]. The properties of the units themselves also are based on similar assumptions [20].

One of the short-comings of many of these models is that they are difficult to analyse mathematically. To address this shortcoming, Chen and Kolokolnikov [1] proposed a "minimal" model of prey-swarm interactions. This model exhibits many of the key aspects of predator-prey interactions, while being as simple as possible, making it amenable to mathematical (and not just numerical) analsyis. The model is

$$\frac{dx_j}{dt} = \frac{1}{N} \sum_{k=1,k\neq j}^{N} \left(\frac{x_j - x_k}{\mid x_j - x_k \mid^2} - a(x_j - x_k) \right) + b\frac{x_j - z}{\mid x_j - z \mid^2}, \tag{1a}$$

$$\frac{dz}{dt} = \frac{c}{N} \sum_{k=1}^{N} \frac{x_k - z}{\mid x_k - z \mid^p}. \tag{1b}$$

Here, x_j are (two-dimensional) prey positions while z is the position of a single predator. The parameter a is associated with prey-prey attraction, b with predator-prey repulsion, c with predator prey interactions, and p loosely with the predator sensitivity to prey. In the paper [1] the authors characterized the steady states of the system and their stability. The reason for particular choices of the nonlinearities becomes clear when one considers the continuum limit of large N, which results in the non-local integro-differential equation model [1]:

[*]Department of Mathematics and Statistics, Dalhousie University, Halifax, NS, Canada, B3H 4R2. Email: `hy495224@dal.ca`.
[†]Department of Mathematics and Statistics, Dalhousie University, Halifax, NS, Canada, B3H 4R2. Email: `tkolokol@gmail.com`.

$$\rho_t(x,t) + \nabla \cdot (\rho(x,t)v(x,t)) = 0; \quad \int_{\mathbb{R}^2} \rho(y,t)dy = 1 \tag{2a}$$

$$v(x,t) = \int_{\mathbb{R}^2} \left(\frac{x-y}{|x-y|^2} - a(x-y) \right) \rho(y,t)dy + b\frac{x-z}{|x-z|^2} \tag{2b}$$

$$\frac{dz}{dt} = c \int_{\mathbb{R}^2} \frac{y-z}{|y-z|^p} \rho(y,t)dy. \tag{2c}$$

The divergence of the velocity then yields

$$\begin{aligned}
\nabla \cdot v &= \int_{\mathbb{R}^2} (\Delta \ln|x-y| - 2a)\, \rho(y,t)dy + b\Delta \ln|x-z| \\
&= \int_{\mathbb{R}^2} (2\pi\delta(x-y) - 2a)\, \rho(y,t)dy + b\delta(x-z) \\
&= 2\pi\rho(x) - 2a, \quad x \neq z
\end{aligned} \tag{3}$$

For a steady state, the velocity is zero so that the swarm density $\rho(x) = a/\pi$ must be constant. Furthermore, any initial conditions evolve to a constant-density state as was shown in [1] (see also [24] and [25]). For reader's convenience, let us repeat the argument here. Define the characteristic curves $X(X_0, t)$ which start from X_0 at $t = 0$:

$$\frac{dX}{dt} = v(X,t); \quad X(X_0, 0) = X_0. \tag{4}$$

Then along the characteristic curves $x = X(X_0, t)$, $\rho(x,t)$ satisfies:

$$\frac{d\rho}{dt} = -(\nabla_x \cdot v)\rho \tag{5}$$

so that from (3) we obtain

$$\frac{d\rho}{dt} = (2a - 2\pi\rho)\rho. \tag{6}$$

It therefore follows that $\rho \to a/\pi$ as $t \to \infty$ along characteristics, provided that initially, $\rho > 0$ at $t = 0$.

It follows that after a transient period, we may replace ρ in (2b) by a constant a/π inside the swarm, and zero outside of the swarm. Equation (2b) then becomes

$$v(x,t) = \frac{a}{\pi} \int_D \left(\frac{x-y}{|x-y|^2} - a(x-y) \right) dy + b\frac{x-z}{|x-z|^2} \tag{7}$$

where D is the extent of the swarm. This is the starting point of this paper. This formula is also utilized to perform numerical simulations of the continuum model by tracking the boundary of the swarm. In this paper, we use this continuum formulation and look more closely at the dynamics discussed by Chen and Kolokolnikov [1] for the predator prey particle model formed using equations (1a) and (1b). We also use the boundary model to consider the case of a single predator traveling on an infinite plane of evenly distributed prey.

2   Boundary evolution method

The particle model (1) or its continuum limit (2) typically produces two relatively well defined boundaries (see Figure 1), one between the predator and the prey, the other enclosing the swarm. To compute these boundaries in the continuum limit (2), we perform a numerical tracking of the boundaries in time by computing the velocity along the boundary using (7). Using divergence theorem, the two-dimensional integral in (7) can be rewritten as an integral along the boundary itself,

$$v(x) = \frac{a}{\pi} \int_{\partial D} \left(-\ln|x-y| + \frac{a}{2}|x-y|^2 \right) \hat{n}dS(y) + b\frac{x-z}{|x-z|^2} \tag{8a}$$

Similarly, substituting $\rho = a/\pi$ into (2c) and using the divergence theorem yields

$$v(z) = \frac{ca}{\pi} \int_{\partial D} \frac{|y-z|^{2-p}}{2-p} \hat{n}dS(y). \tag{8b}$$

2

(a)   (b)
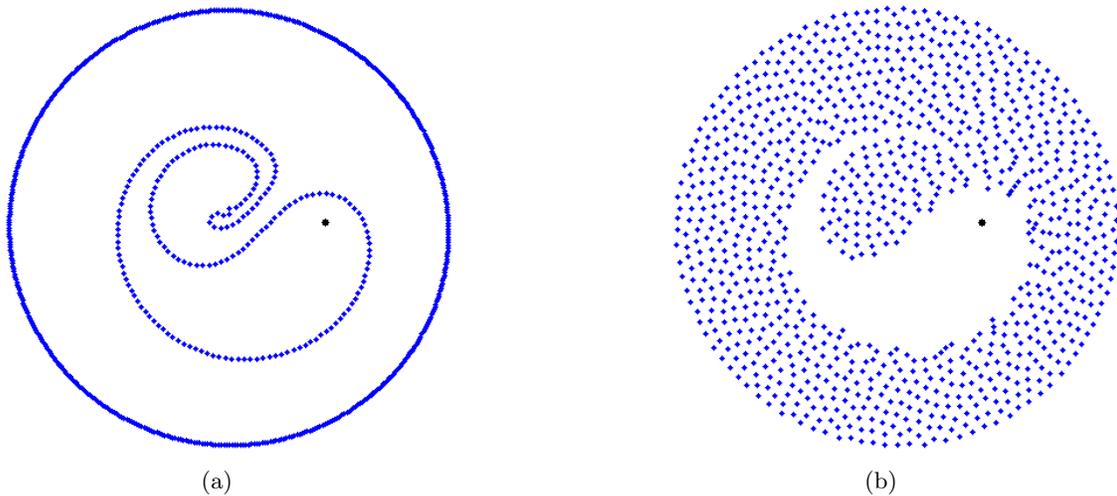
Figure 1: Comparison between (a) the boundary model (8) and (b) the full particle model (1). Parameter for both (a) and (b) are $c = 1.5, a = 1, b = 0.2$. For the figure (a), 200 points were used for the inner boundary and 500 for the outer boundary. In (b), a total of 1000 particles were used in (1).

By discretizing the inner and outer boundaries, the integral in (8a) is approximated numerically for each point on the boundary. The boundary D and the predator location z are then evolved according to the velocities thus computed.

We first used the standard Forward Euler method to update to points on the boundary. Numerically, we found that this computation was often unstable, regardless of the choice of time step Δt. The is because the points along the boundary tend to cluster together as time evolves. This is a result of the points being pushed back along the boundary and aggregating at the tail. As a remedy we introudced reparameterization based on arc length at every time step.

To reparameterize a curve based on arc length, we introduced the arclength monitor function, $M(i)$ such that $M(0) = 0$ and $M(i + 1) = M(i) + |x_i - x_{i-1}|$. We then reparametrize the curve such that M is equividistributed. The following self-contained Matlab code fragment illustrates the details:

```
% Input: complex vector x representing a curve. For exmaple:
x=exp(linspace(0,1,10).^2*1i*pi);

% Output: curve y reparametrized by arclength

n=numel(x);
monitor = x*0;
for i=2:n
   monitor(i)=monitor(i-1)+abs(x(i)-x(i-1));
end;
L=monitor(end);
eq1=linspace(0,L,n);
eq2=interp1(monitor, linspace(0,n,n), eq1);
y=interp1(linspace(0,n,n), x, eq2);

clf; plot(x, '.-b'); hold on; plot(y, '.-r'); axis equal;
```

This reparametrization stabilized the numerics. Figure 1 shows a good agreement between the particle model and the boundary evolution method. An important difference here is the tail. In the particle model, the tail merges with the boundary creating an "island" in the middle. On the other hand, in the boundary model the tail curls in on itself. The tail itself that forms extends and shortens with time, similar to the case we see in Figure 7 of section 3.2. A possible future work is to extend the boundary model to allow the merging of the boundaries and formation of "islands".

3   Infinite swarm limit

In [1], it was shown that the model (2) admits a steady state for which the swarm boundary consists an annulus whose inner radius R_1 and outer radius R_2 are given by

$$R_1 = \sqrt{\frac{b}{a}} \qquad R_2 = \sqrt{\frac{1+b}{a}} \tag{9}$$

and with the predator located at the center of this boundary. In the double limit $a \to 0$ and $b = O(a)$, note that $R_2 \to \infty$ while R_1 remains $O(1)$. Thus the exterior boundary becomes infinite while the interior boundary remains finite in size.

Taking the limit $a \to 0$ in (8a) and discarding the $O(a^2)$ terms as well as the exterior boundary, we obtain

$$v(x) = \frac{1}{\pi} \int_{-\partial D_i} -a \ln|x - y| \, \hat{n} dS(y) + b\frac{x - z}{|x - z|^2} \tag{10}$$

where $-\partial D_i$ denotes an interor boundary, traversed clockwise. By rescaling space we may take without loss of generality $a = b$. By rescaling time $t = a\hat{t}$ and dropping the hat, the equation for velocity then becomes

$$v(x) = \frac{1}{\pi} \int_{\partial D_i} \ln|x - y| \, \hat{n} dS(y) + \frac{x - z}{|x - z|^2}. \tag{11}$$

The swarm has an interior boundary ∂D_i while the exterior boundary is assumed to be arbitrary large. We refer to (11) as the *infinite swarm limit model*. It must be coupled with some law of motion for the predator z. The simplest such motion is to assume that z moves at a constant speed along a straight line. This is studied in section 3.1. A predator moving in a circle is studied in 3.2. Even in this simplest of settings, complex boundary shapes can be observed for which we do not know any closed-form solutions. Furthemore, when the predator is moving sufficiently fast, we observe a formation of an infinite tail behind the inner swarm boundary.

3.1   Predator moving in straight line

To investigate the properties of a single boundary model, first consider the case of z moving in a straight line at a constant speed, ω. For simplicity let z move along the horizontal axis. Thus, the movement of z is modeled by the following equation

$$z = \omega t \tag{12}$$

To aid in comparison of these graphs between different values of ω consider looking at the movement of z in a moving frame such that z appears stationary. Again, for convenience set z at the origin. This is done by making the following change of coordinates

$$x = \tilde{x} + \omega t \tag{13}$$

so that $v(x) = dx/dt = d\tilde{x}/dt + \omega = v(\tilde{x}) + \omega$, and $z = 0$. Then the infinite swarm model (11) becomes, after dropping the tildes,

$$v(x) = \frac{1}{\pi} \int_{\partial D_i} \ln|x - y| \, \hat{n} dS(y) + \frac{x}{|x|^2} - \omega \tag{14}$$

Figure 2 shows the the evolution of the boundary for ω equal to 0.2, 0.4, and 0.6. For small ω, after a short transient time, the boundary shape converges to the steady state in the translational frame for which v in (14) is zero for x along ∂D_i. However as ω is increased, a tail starts to form at the back of the boundary. This tail appears to grow indefinitely as t is increased, as illustrated in Figure 3.

The bifurcation appears to occur when ω is increased past some critical value $\omega = \omega_c$. Numerical testing showed this value is approximately 0.25. While Figure 3 shows the tail at specific times, it is important to note that this tail does not appear to reach a stationary state, but rather continually lengthens.

The tail itself is reminiscent of the tail seen in the particle model formed by (1a) and (1b) as well as the one that formed in the case of z moving in a circle in section 3.2 below. It is possible that the rotating nature of these other cases prevent the tail from forming, as it would be force to cross its own boundary otherwise. Furthermore, we note the solution found in a model by Mogilner and Edelstein-Keshet [26], which indicated a similar infinite tail of prey would form.
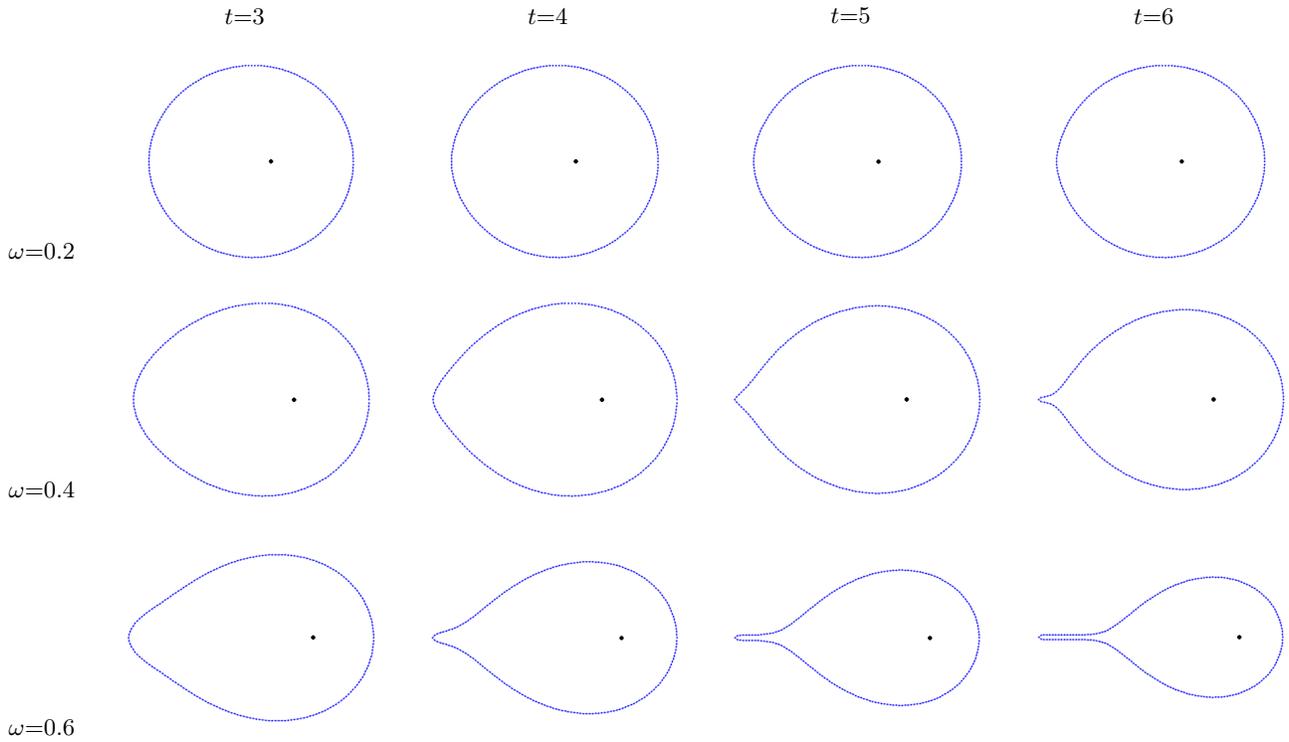
Figure 2: Stationary plots using (14) showing the effect of different values of ω over time. Parameters are t and ω as given. While ω=0.2 reaches a stationary state, $\omega = 0.4$ and $\omega = 0.6$ continue to grow with time

Further numerical simulations show that there is a saddle point (see Figure 4) that lies on x-axis to the left of the boundary for values of ω lower than ω_c. As the value of ω increases towards ω_c, this saddle point crosses the boundary, inducing a topological change in the shape of the swarm.
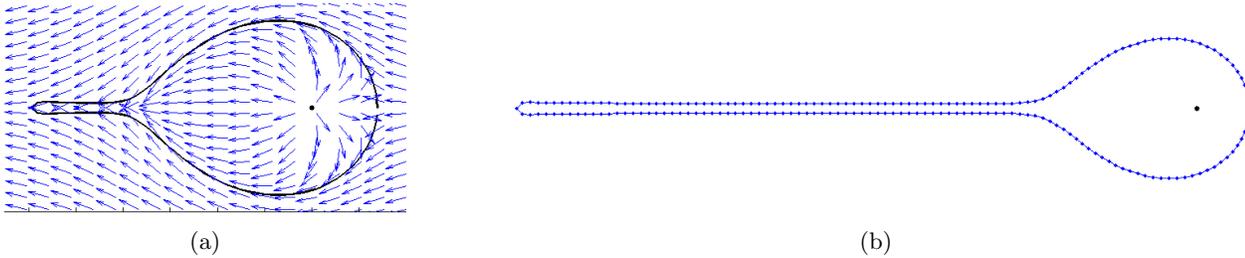
Figure 3: Model using (14) to show the tail that begins to form as time increases for larger values of ω. (a) Parameters are $n = 100$, $t = 8.0$, and $\omega = 0.5$. (b) Parameters are $n = 200$, $t = 24.0$, and $\omega = 0.5$.

There is a secondary bifurcation that appears as ω is increased further, well beyond $\omega_c \approx 0.25$. For increasingly large ω, the predator location starts to approach the right boundary of the swarm. As we further increase the value of ω, the distance between the predator to the prey decreases, as illustrated in in figures 2, 5. At a certain point, ω becomes large enough that the predator is able to catch the prey. To quantify this value of ω, which we'll denote as ω_{catch}, we'll consider it to be the smallest value of omega for which the the distance between the predator and the closest prey falls below 0.05. In finding ω_{catch} we must consider two factors: n, the number of points with which we model the boundary, and dt, our timestep. While n is able to be changed without greatly varying the results, dt must be made small enough. Chiefly, dt produces stable results when it is ≤ 0.001. With $dt = 0.001$ and $n = 200$ the value of $\omega_{catch}$is approximately 19.2. Beyond this value, the numerics start to become unstable and quickly break down.

<div align="center">(a)</div>

<div align="center">(b)</div>
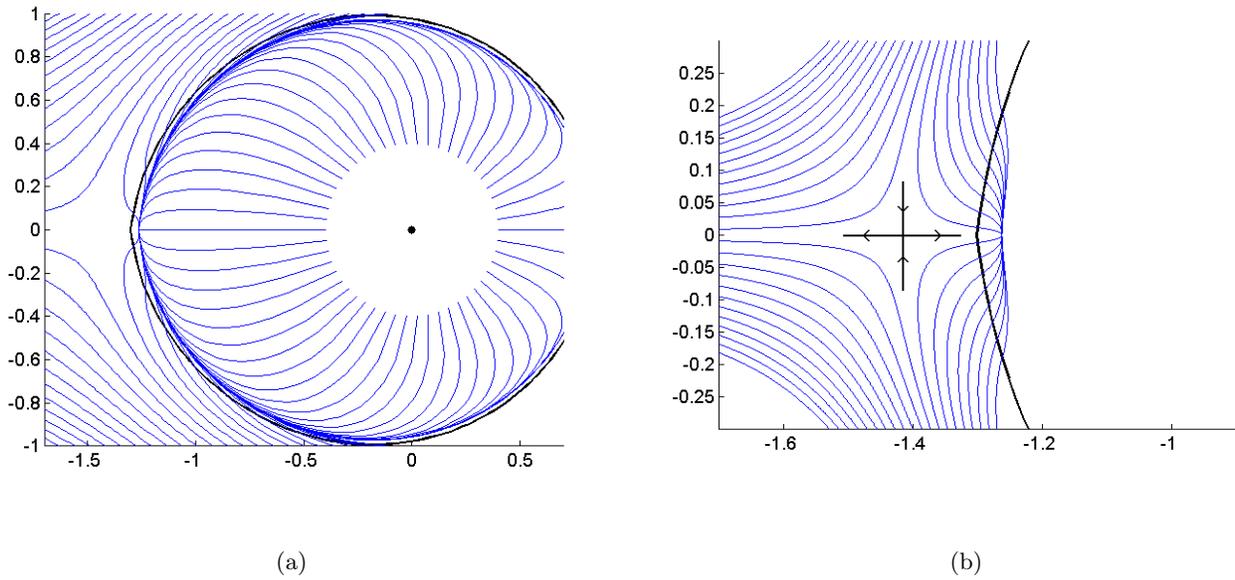
Figure 4: Orbit plots using (14). Parameters are $n = 200$ and $\omega = 0.2$. The location of the saddle point and end associate with this ω are -1.4158 and -1.3019 respectively. (a) Orbits around whole model. (b) Orbits around end and saddle point.
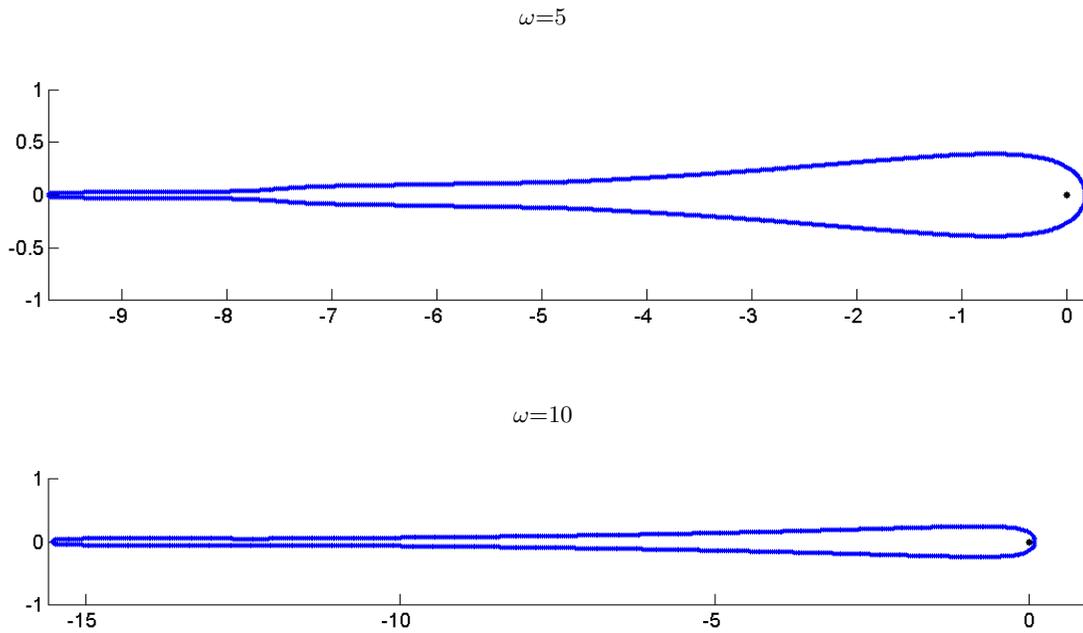
Figure 5: Plots of (14) for larger values of omega as given. Parameters are $t = 1.5$ and $n = 1000$. The distance between the predator and the closest prey is 0.1737 and 0.0903 for $\omega = 5$ and $\omega = 10$ respectively.

3.2 Predator moving in a circle

We now consider a predator moving in a circle within the infinite plane of prey. Again, it is possible to use (11) as a model for the velocity of the prey, while the movement of z can be determined using the following

$$z = Re^{i\omega t} \tag{15}$$

Here, R is the radius of the circle traveled by z and ω is the angular velocity of z. Just as in the case of z moving in a straight line, we change to a moving frame. Consider a change to a rotating frame where z is stationary at $z = R$. Again, this is modeled using a change of coordinates, as follows

$$x = \tilde{x}e^{i\omega t} \tag{16}$$

and leads us to the following model

$$v(x) = \frac{1}{\pi} \int_{\partial D_i} \ln|x - y| \,\hat{n}dS(y) + \frac{x - R}{|x - R|^2} - i\omega x. \tag{17}$$
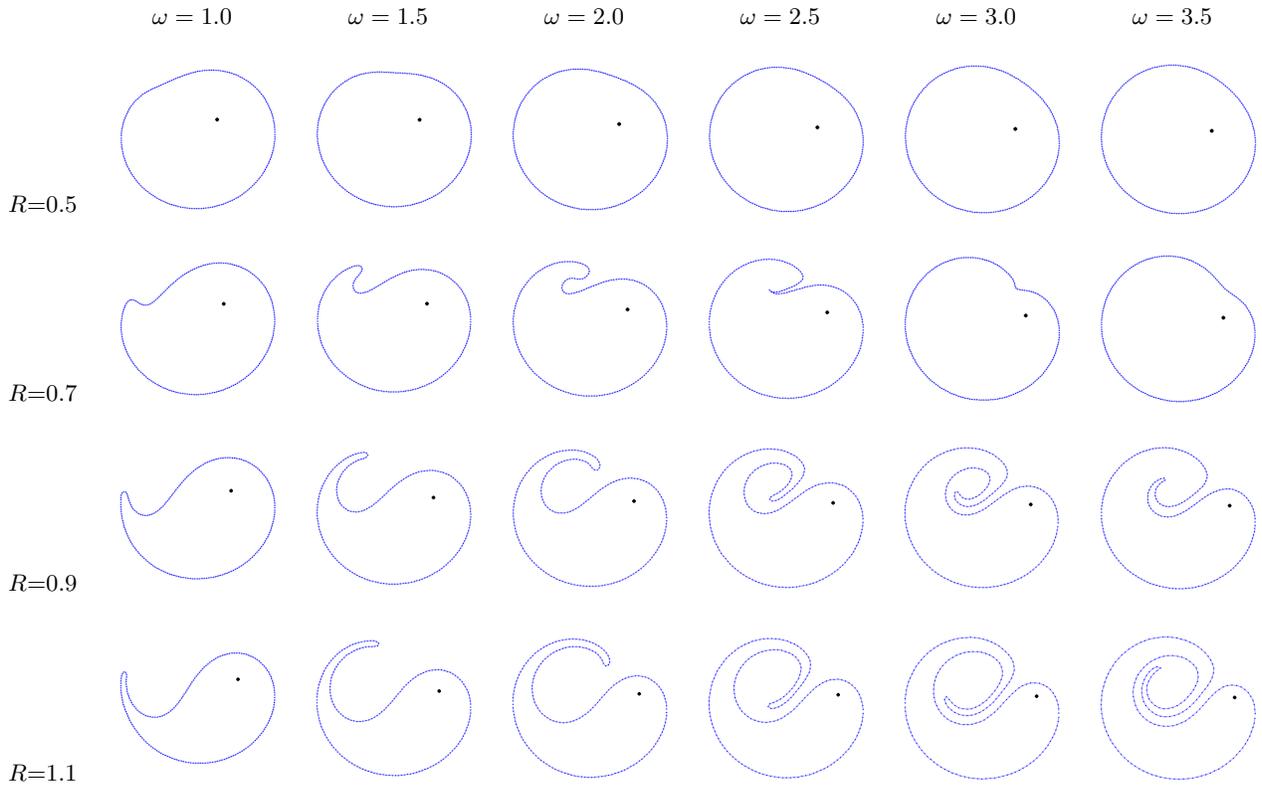
Figure 6: Plots of (17) for different values ω and R. Models were run to a stationary state with x_1 fixed to remain at the rightmost point. For each R the previous stationary state was used as the initial setup for the proceeding value of ω. Parameters are $n = 200$ and ω and R as given.

Figure 6 shows the variety of the steady states (in the rotational frame) that can occur for various values of R and ω. When R is small, such as $R = 0.5$, the steady state seems to be influenced very little by a changing ω, and maintain a relatively circular boundary. While larger values of R, such as $R = 0.9$ show great dissimilarities in the boundaries formed by different omegas. In many sets of parameters, a tail forms without ever stabilizing and repeatedly decreases and increases in length. An example of this is visible in Figure 7.

In order to achieve a more stable figure for the different R and ω combinations, the first point on the boundary, x_1, is fixed to stay at the rightmost point in the diagram after each reparametrization. With this modification, most parameters allow the boundary to be unchanging in shape over time. As well, this allows us to more easily visualize the effects different combinations of R and ω on model (17). Whereas low values of R and ω produce relatively a circular boundary, the model begins to grow a tail and to increase in complexity as we increase R and ω. In
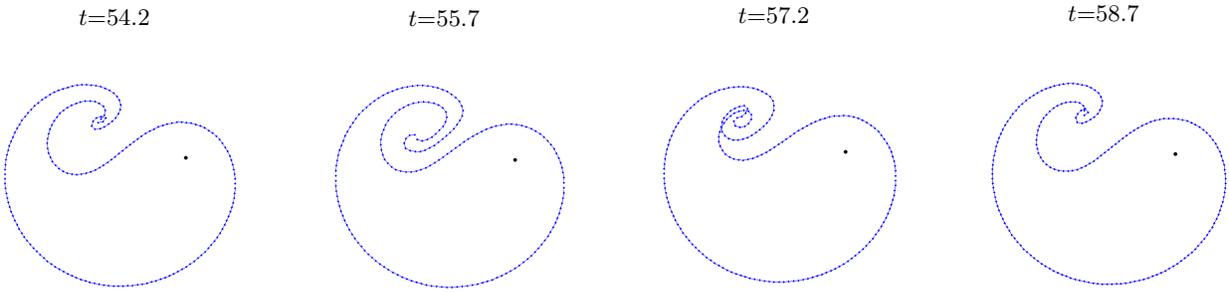
Figure 7: Moving tail for model (14). Parameters are $n = 200$, $\omega = 2.0$, $R = 0.9$, and time as given.

particular, having $R = 0.7$ and $\omega = 2.5$ causes the boundary to slide back and forth, so that a stable rotating state is never reached. In other cases, the tail continues to grow and wraps around the itself again, forming a second boundary. This is seen in Figure 8. With lower values of ω the formation of a second boundary is often preventible by slowly increasing ω towards its desired value.
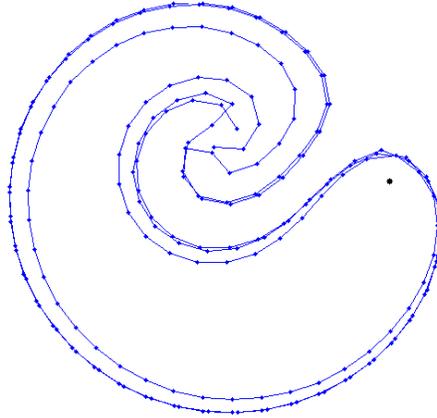
Figure 8: Parameters are $n = 200$, $R = 0.7$, $\omega = 6.0$. Still taken at $t = 50$ with ω equal to the minimum of $2 + 0.1 * t$ and 6.0.

To more closely examine what is happening in the cases of (17) where the dynamics become complex, we examine the vector fields around the boundary plots. An example of this is shown in Figure 9. In this figure, we see a distinct "whirlpool" in the vector field that causes the tail to curl around.

A larger picture of this is visible in Figure 10. Figure 10 also shows a distinct saddle point like spot. In the case presented the point sits inside the boundary. In the case of a moving tail we see the point along the boundary, effectively pushing points toward it vertically and away from it horizontally along the boundary.

In the case of where x_1 is not fixed, an evident difference in this model is that the gap in the boundary between x_1 and x_n is not able to move to the end of the tail. In the case of a fluctuating tail, this seemingly allows the tail to grow long, and causes it to run into its own boundary. When it does so it is expelled back outside, and the cycle repeats itself. The vector field itself seems to evolve little.

4   Discussion and extensions

In this paper we have investigated the dynamics and the steady states of the predator-swarm model (1) introduced in [1]. The advantage of this model is that in the large N limit, the swarm density is constant, which makes it possible to describe the dynamics purely in terms of the evolution of the boundary of the swarm. We implemented
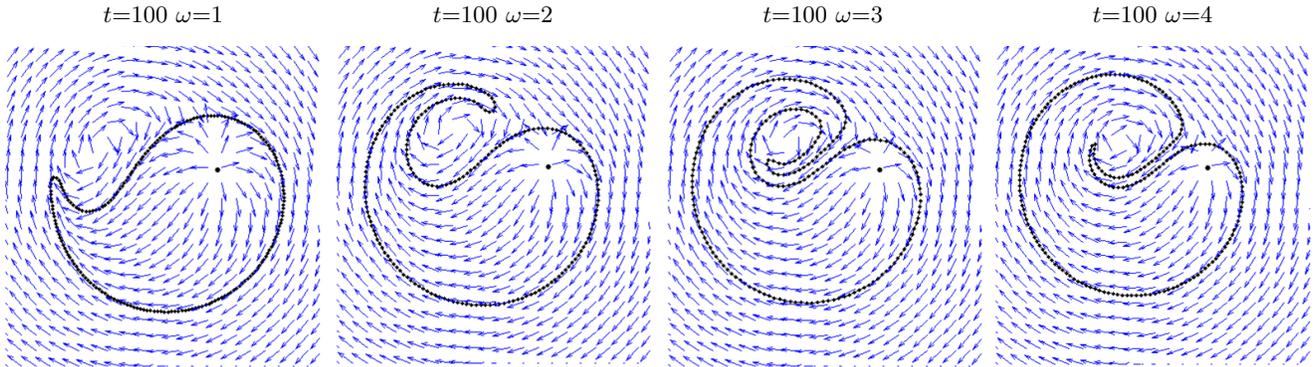
Figure 9: Vector field plots of (17) with $\omega = 0.01t$, $R = 9$, and x_1 fixed to remain at the rightmost point. Parameters were $n = 200$ and t as given.

(a)

(b)
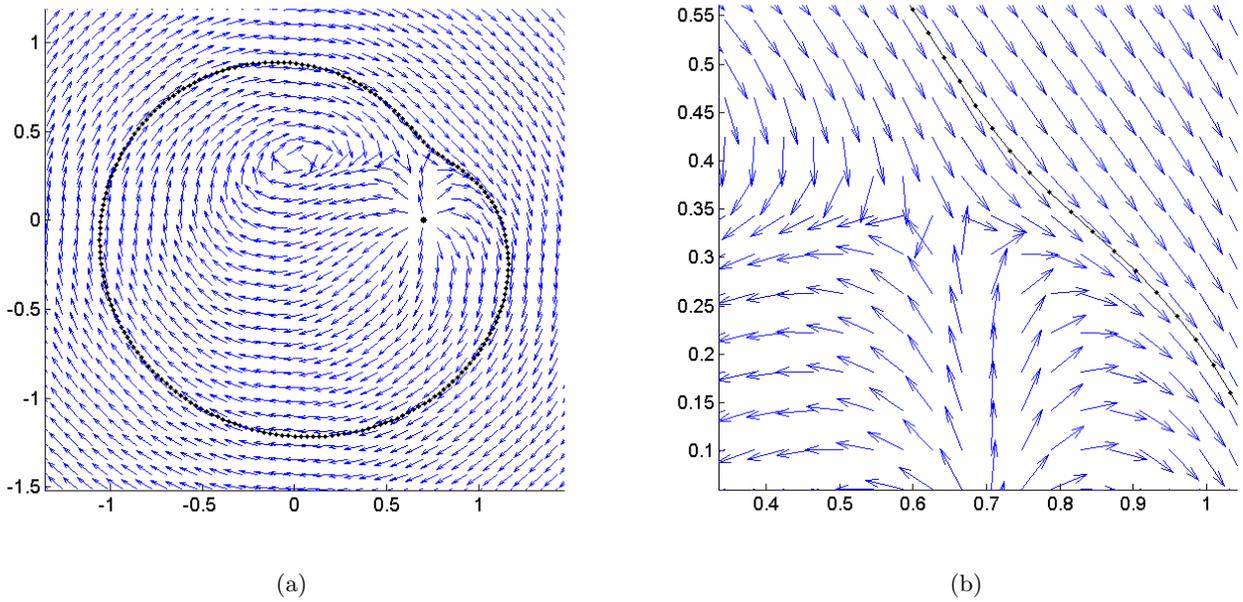
Figure 10: Vector field plot of the steady state for (17) with $\omega = 3.5, R = 0.7$ and $n = 200$. (a) Full image. (b) Close up of vector dynamics.

a numerical method to track the boundary, and investigated the resulting steady states in rotating frame. We then considered a limiting case of a predator moving inside a sea of infinite swarm. In this case, only the interior boundary needs to be tracked. We considered two cases: a predator moving along a straight line, and a predator moving in a circle. The former is particularly simple, since there is only one effective parameter, which is the speed of the predator. Even in this simplified setting, we showed that the interior boundary forms an infinite tail as the speed of the predator is increased beyond a certain threshold. In the case of a predator moving in a circle, the steady state exhibits a very rich structure with multipe transitions depending on the radius and angular velocity of the predator.

Our numerical investigations pose many open questions. For example, in the case of a predator moving in a straight line, is it possible to find a closed-form solution for the shape of the steady state? We demonstrated numerically that the appearance of an infinite tale is related to topological changes as a saddle point crosses the swarm boundary. Can this be studied analytically? These and related questions pose challenging problems for future study.

References

[1] Y. Chen, T. Kolokolnikov, A minimal model of predator–swarm interactions, Journal of The Royal Society Interface 11 (94) (2014) 20131208.

[2] Y. Katz, K. Tunstrøm, C. C. Ioannou, C. Huepe, I. D. Couzin, Inferring the structure and dynamics of interactions in schooling fish, Proceedings of the National Academy of Sciences 108 (46) (2011) 18720–18725.

[3] U. Lopez, J. Gautrais, I. D. Couzin, G. Theraulaz, From behavioural analyses to models of collective motion in fish schools, Interface Focus (2012) rsfs20120033.

[4] A. Okubo, D. Grünbaum, L. Edelstein-Keshet, The dynamics of animal grouping, in: Diffusion and ecological problems: modern perspectives, Springer, 2001, pp. 197–237.

[5] C. W. Reynolds, Flocks, herds and schools: A distributed behavioral model, ACM SIGGRAPH Computer Graphics 21 (4) (1987) 25–34.

[6] C. Huepe, G. Zschaler, A.-L. Do, T. Gross, Adaptive–network models of swarm dynamics, New Journal of Physics 13 (7) (2011) 073022.

[7] J. Buhl, G. A. Sword, S. J. Simpson, Using field data to test locust migratory band collective movement models, Interface focus (2012) rsfs20120024.

[8] L. Edelstein-Keshet, Mathematical models of swarming and social aggregation, in: Proceedings of the 2001 International Symposium on Nonlinear Theory and Its Applications, Miyagi, Japan, 2001, pp. 1–7.

[9] A. J. Bernoff, C. M. Topaz, A primer of swarm equilibria, SIAM Journal on Applied Dynamical Systems 10 (1) (2011) 212–250.

[10] V. Zhdankin, J. Sprott, Simple predator-prey swarming model, Physical Review E 82 (5) (2010) 056209.

[11] G. Flierl, D. Grünbaum, S. Levins, D. Olson, From individuals to aggregations: the interplay between behavior and physics, Journal of Theoretical Biology 196 (4) (1999) 397–454.

[12] R. Lukeman, Y.-X. Li, L. Edelstein-Keshet, Inferring individual rules from collective behavior, Proceedings of the National Academy of Sciences 107 (28) (2010) 12576–12580.

[13] P. Kareiva, G. Odell, Swarms of predators exhibit "preytaxis" if individual predators use area-restricted search, The American Naturalist 130 (2) (1987) pp. 233–270.

[14] A. Ordemann, G. Balazsi, F. Moss, Pattern formation and stochastic motion of the zooplankton daphnia in a light field, Physica A: Statistical Mechanics and its Applications 325 (12) (2003) 260 – 266, stochastic Systems: From Randomness to Complexity.

[15] A. Eriksson, M. N. Jacobi, J. Nyström, K. Tunstrøm, Determining interaction rules in animal swarms, Behavioral Ecology 21 (5) (2010) 1106–1111.

[16] S. Nishimura, T. Ikegami, Emergence of collective strategies in a prey-predator game model, Artificial Life 3 (4) (1997) 243–260.

[17] M. Higashitani, A. Ishigame, K. Yasuda, Particle swarm optimization considering the concept of predator-prey behavior, in: Evolutionary Computation, 2006. CEC 2006. IEEE Congress on, 2006, pp. 434–437.

[18] M. M. Molina, M. A. Moreno-Armendriz, J. C. S. T. Mora, On the spatial dynamics and oscillatory behavior of a predator-prey model based on cellular automata and local particle swarm optimization, Journal of Theoretical Biology 336 (0) (2013) 173 – 184.

[19] A. Silva, A. Neves, E. Costa, An empirical comparison of particle swarm and predator prey optimisation, in: Artificial Intelligence and Cognitive Science, Springer, 2002, pp. 103–110.

[20] A. Deutsch, G. Theraulaz, T. Vicsek, Collective motion in biological systems, Interface Focus 2 (6) (2012) 689–692.

[21] J. K. Parrish, L. Edelstein-Keshet, Complexity, pattern, and evolutionary trade-offs in animal aggregation, Science 284 (5411) (1999) 99–101.

[22] D. J. Sumpter, R. P. Mann, A. Perna, The modelling cycle for collective animal behaviour, Interface focus (2012) rsfs20120031.

[23] A. Rozenfeld, E. Albano, Study of a lattice-gas model for a preypredator system, Physica A: Statistical Mechanics and its Applications 266 (14) (1999) 322 – 329.

[24] R. C. Fetecau, Y. Huang, T. Kolokolnikov, Swarm dynamics and equilibria for a nonlocal aggregation model, Nonlinearity 24 (10) (2011) 2681.

[25] A. L. Bertozzi, T. Laurent, F. Léger, Aggregation and spreading via the newtonian potential: the dynamics of patch solutions, Mathematical Models and Methods in Applied Sciences 22 (supp01).

[26] A. Mogilner, L. Edelstein-Keshet, A non-local model for a swarm, Journal of Mathematical Biology 38 (6) (1999) 534–570.